PCCP

Directed Gas Phase Preparation of Ethynylallene ($H_2CCCHCCH$; X^1A') via the Crossed Molecular Beam Reaction of the Methylidyne Radical (CH; $X^2\Pi$) with Vinylacetylene ($H_2CCHCCH$; X^1A')

Journal:	*Physical Chemistry Chemical Physics*
Manuscript ID	CP-ART-09-2022-004081.R1
Article Type:	Paper
Date Submitted by the Author:	19-Oct-2022
Complete List of Authors:	He, Chao; University of Hawai'i at Manoa, Department of Chemistry Yang, Zhenghai; University of Hawai'i at Manoa Doddipatla, Srinivas; University of Hawai'i at Manoa, Department of Chemistry Thomas, Aaron; University of Hawaii, Chemistry Kaiser, Ralf; University of Hawaii, Galimova, Galiya; Florida International University Mebel, Alexander; Florida International University, Chemistry and Biochemistry Fujioka, Kazuumi; University of Hawai'i at Manoa, Chemistry Sun, Rui; University of Hawai'i at Manoa, Chemisty

Directed Gas Phase Preparation of Ethynylallene ($H_2CCCHCCH$; X^1A') via the Crossed Molecular Beam Reaction of the Methylidyne Radical (CH; $X^2\Pi$) with Vinylacetylene ($H_2CCHCCH$; X^1A')

Chao He,[a] Zhenghai Yang,[a] Srinivas Doddipatla,[a] Aaron M. Thomas,[a] Ralf I. Kaiser[a]*

[a] *Department of Chemistry, University of Hawai'i at Mānoa, Honolulu, HI 96822, USA*

Galiya R. Galimova,[b] Alexander M. Mebel,[b]*

[b] *Department of Chemistry and Biochemistry, Florida International University, Miami, Florida 33199, USA*

Kazuumi Fujioka,[a] Rui Sun[a]*

Department of Chemistry, University of Hawai'i at Mānoa, Honolulu, HI 96822, USA

Corresponding Author Prof. Dr. Ralf I. Kaiser: ralfk@hawaii.edu

Corresponding Author Prof. Dr. Alexander M. Mebel: mebela@fiu.edu

Corresponding Author Prof. Rui Sun: ruisun@hawaii.edu

Abstract

The gas-phase bimolecular reaction of the methylidyne (CH; $X^2\Pi$) radical with vinylacetylene ($H_2CCHCCH$; X^1A') was conducted at a collision energy of 20.3 kJ mol^{-1} under single collision conditions exploiting the crossed molecular beams experimental results merged with ab initio electronic structure calculations and ab initio molecular dynamics (AIMD) simulations. The laboratory data reveals that the bimolecular reaction proceeds barrierlessly via indirect scattering dynamics through long-lived C_5H_5 reaction intermediate(s) ultimately dissociating to C_5H_4 isomers along with atomic hydrogen with the latter predominantly originated from the vinylacetylene reactant as confirmed by the isotopic substitution experiments in the D1-methylidyne–vinylacetylene reaction. Combined with ab initio calculations of the potential energy surface (PES) and statistical Rice–Ramsperger–Kassel–Marcus (RRKM) calculations, the experimental determined reaction energy of -146 ± 26 kJ mol^{-1} along with the distribution minimum of $T(\theta)$ at 90° and isotopic substitution experiments suggests ethynylallene (**p1**; $\Delta rG = -230 \pm 4$ kJ mol^{-1}) as the dominant product. The ethynylallene (**p1**) may be formed with extensive rovibrational excitation, which would result in a lower maximum translational energy. Further, AIMD simulations reveal that the reaction dynamics leads to **p1** (ethynylallene, 75 %) plus atomic hydrogen with the dominant initial complex being **i1** formed by methylidyne radical addition to the double C=C bond in vinylacetylene. Overall, combining the crossed molecular beams experimental results with ab initio electronic structure calculations and ab initio molecular dynamics (AIMD) simulations, ethynylallene (**p1**) is expected to represent the dominant products in the reaction of the methylidyne (CH; $X^2\Pi$) radical with vinylacetylene ($H_2CCHCCH$; X^1A').

1. INTRODUCTION

The investigation on the formation mechanisms of polycyclic aromatic hydrocarbons (PAHs) – organic molecules composed of fused aromatic rings – has caught attention of the physical (organic), astrochemistry, and theoretical chemistry communities over the last few decades as a result of the importance of PAH-like species in various environments, such as combustion flames, interstellar media, and planetary atmospheres.[1-10] In deep space, spectroscopic features of PAH related molecules including alkylated, ionized, (de)hydrogenated and protonated counterparts[11-16] have been inferred from the diffuse interstellar bands (DIBs) and unidentified infrared (UIRs) bands within the wavelength range of 200–400 nm (ultraviolet) and 3–20 mm (infrared).[2-4, 17-22] Further, PAHs and their derivatives, which contribute up to 20% of the galactic carbon budget,[23] are potential crucial intermediates and nucleation sites that ultimately yield carbonaceous nanoparticles (‘‘interstellar grains’’).[4, 21, 22, 24-26] In terrestrial environment, largely produced in the incomplete hydrocarbon combustion, PAHs are believed to be the key precursors to unwanted soot formation[5] resulting to combustion inefficiency and a public health hazard.[6-8] Hence, the understanding of the fundamental reaction mechanisms in the synthesis of PAHs and their precursors in combustion systems as well as deep space will provide significant insights into how complex aromatic molecules and even graphenes and fullerenes are formed.[27-37]

Odd-carbon radicals tend to be resonantly stabilized free radicals (RSFRs) and have been proposed to promote PAH formation and growth in combustion flames.[38, 39] There is a consensus that the chemistry of cyclopentadienyl (c-C_5H_5) radical plays a significant role in the formation of naphthalene and phenanthrene and, consequently, in the formation of PAHs.[1, 40-43] Nevertheless, the origin of cyclopentadienyl (c-C_5H_5) along with its structural isomers has remained elusive. Gabriel da Silva studied the C_5H_5 potential energy surface (PES) via the reaction of the propargyl radical (C_3H_3) with acetylene (C_2H_2) from *ab initio* calculations.[44] The addition of acetylene (C_2H_2) to the end of the propargyl radical (C_3H_3) leads to the initial complexes 1-penten-4-ynyl (HCC H_2CCHCH•) and 1,3,4-pentatrienyl (H_2CCCHCHCH•) via similar barriers, about 59 kJ mol^{-1} above the separated reactants.[44] The acyclic C_5H_5 isomers may isomerize to cyclopentadienyl (*c*-C_5H_5) with the highest transition state located 64 kJ mol^{-1} above the separated reactants.[44] The chemical kinetic models revealed that the yield of the *l*-C_5H_5 and *c*-C_5H_5 isomers are similar at temperatures and pressures relevant to combustion processes.[44] Crossed molecular beam studies were performed on the reaction of (D-)ethynyl radical (C_2H/C_2D) with methylacetylene

(CH_3CCH)[45, 46] under single collision conditions. Combining the experimental findings with a theoretical study of C_5H_5 PES, methyldiacetylene (CH_3CCCCH) was revealed as the dominant atomic hydrogen loss product along with a smaller contribution of ethynylallene ($H_2CCCHCCH$). The reactions of the ethynyl radical (C_2H) with allene (H_2CCCH_2) were explored both experimentally[47] and computationally.[48] Ethynylallene ($H_2CCCHCCH$) emerged as the major product, with 1,4-pentadiyne ($HCCH_2CCCH$) contributing up to 20%.[47, 48] Later on, Jamal and Mebel conducted systematic studies via ab initio CCSD(T)/cc-pVTZ//B3LYP/6-311G** calculations of the C_5H_5 PES investigating the reaction mechanism of ethynyl radical (C_2H) with C_3H_4 isomers, allene (H_2CCCH_2) and methylacetylene (CH_3CCH).[49] For the C_2H-H_2CCCH_2 system, 1,4-pentadiyne (56–63%), ethynylallene (22–24%), and pentatetraene (10–15%) are expected to be prominent atomic hydrogen loss products.[49] On the contrary, for the C_2H-CH_3CCH reaction, the methyl (CH_3) loss channel which leads to diacetylene may contribute up to 21–61%, while the other important products include methyldiacetylene (27–56%) and ethynylallene (11–22%).[49]

The aforementioned studies revealed that the reaction mechanisms involved in the formation of C_5H_x (x = 4, 5) isomers are very complex and far from being resolved. Here, we provide a unique glimpse into the chemistry of distinct C_5H_x (x = 4, 5) isomers by unraveling their gas-phase preparation under single-collision conditions via the bimolecular reaction of the methylidyne radical (CH; $X^2\Pi$) with vinylacetylene ($H_2CCHCCH$; X^1A'). The combination of the experimental data with electronic structure calculations as well as ab initio molecular dynamics simulations on the C_5H_5 PES identified that ethynylallene (**p1**) along with atomic hydrogen may be formed under single-collision conditions. Since in crossed molecular beam studies, the nascent products 'fly away' from the collision center, they form without successive reactions in the gas-phase.[50, 51]

2. EXPERIMENTAL & COMPUTATIONAL

2.1. EXPERIMENTAL

The elementary gas-phase reaction of the (D1-)methylidyne (CH/CD; $X^2\Pi$) radical with vinyl-acetylene ($H_2CCHCCH$; X^1A') was carried out under single-collision conditions in a universal crossed molecular beams machine at the University of Hawaii.[52] In the primary source chamber, a pulsed supersonic beam of the (D1-)methylidyne (CH/CD) radicals was generated by photodissociation (COMPex 110, Coherent, Inc; 248 nm; 30 Hz) of (D1-)bromoform

($CHBr_3$/$CDBr_3$, Aldrich Chemistry, ≥ 99 %) seeded in helium (99.9999 %; AirGas).[53] After passing through the skimmer, the methylidyne radicals were velocity-selected by a four-slot chopper wheel yielding a peak velocity v_p of 1867 ± 13 m s^{-1} and a speed ratio S of 12.6 ± 0.4 (Table 1). The rotational temperature of the methylidyne radicals was determined to be 14 ± 1 K utilizing laser-induced fluorescence.[54] In the secondary source chamber, a supersonic beam of 5 % vinylacetylene seeded in argon (99.9999 %; AirGas) with v_p = 642 ± 20 m s^{-1} and S = 26.0 ± 1.0 (Table 1) crossed the methylidyne radicals perpendicularly in the interaction region of the scattering chamber resulting in a collision energy (E_C) of 20.3 ± 0.3 kJ mol^{-1} and a center of mass angle (Θ_{CM}) of 54.0 ± 0.9°. Vinylacetylene was synthesized in house.[55] The neutral reaction products entering the detector were ionized via electron impact ionization (80 eV, 2.0 mA),[56] mass-filtered according to their mass-to-charge ratio (m/z) utilizing a quadrupole mass spectrometer (QMS, Extrel, QC 150), and eventually recorded by a Daly-type ion counter.[57] The detector is housed within a triply differentially pumped (6×10^{-12} Torr), rotatable chamber that allows the collection of angularly-resolved time-of-flight (TOF) spectra in the plane defined by both reactant beams. To obtain the information on the reaction dynamics, a forward-convolution method was used to transform the laboratory frame (LAB) data into the center of mass frame (CM);[58, 59] this iterative method exploits a user-defined CM translational energy $P(E_T)$ and angular $T(\theta)$ flux distributions, which were varied until a best fit of the laboratory-frame TOF spectra and angular distributions was achieved. These functions define the reactive differential cross-section $I(u, \theta) \sim P(u)\times T(\theta)$ *with* the CM scattering angle θ and CM velocity u. The error ranges of the $P(E_T)$ and $T(\theta)$ functions were determined within the 1σ limits of the corresponding laboratory angular distribution and beam parameters (beam velocity and angular spread, beam velocity) while maintaining a good fit of the laboratory TOF spectra.

2.2. COMPUTATIONAL

2.2.1. AB INITIO ELECTRONIC STRUCTURE CALCULATIONS

Geometries of all species involved in various chemical reactions accessing the C_5H_5 PES including reactants, intermediates, transition states, and products were optimized using the doubly hybrid density functional theory (DFT) B2PLYPD3 method[60-62] with Dunning's correlation-consistent cc-pVTZ basis set (4).[63] Then, vibrational frequencies for all optimized structures were computed using the same method to evaluate zero-point vibrational energy corrections (ZPE) and

to be utilized in rate constant calculations. Single-point energies were rectified using the explicitly correlated coupled clusters approach with single and double excitations with perturbative treatment of triple excitations, CCSD(T)-F12,[64, 65] with Dunning's cc-pVQZ-f12 basis set. The anticipated accuracy of the CCSD(T)-F12/cc-pVQZ-f12//B2PLYPD3/cc-pVTZ + ZPE (B2PLYPD3/cc-pVTZ) relative energies is typically within 4 kJ mol^{-1} or better.[66] The Gaussian 16 [67] and MOLPRO 2021[68] program packages were used for the ab initio calculations. Energy-dependent rate constants of all unimolecular reaction steps on the C_5H_5 PES following initial addition of methylidyne radical to vinylacetylene were computed using Rice-Ramsperger-Kassel-Marcus (RRKM) theory.[69, 70] Here, a rate constant $k(E)$ at an internal energy E for a unimolecular reaction A*→A$^{\#}$→P was evaluated as

$$k(E) = \frac{\sigma W^{\#}(E - E^{\#})}{h \quad \rho(E)}$$

where σ is the reaction path degeneracy, h is Planck's constant, $W^{\#}(E–E^{\#})$ is the total number of states for the transition state A$^{\#}$ with a barrier $E^{\#}$, $\rho(E)$ is the density of states of the energized reactant molecule A*, and P denotes products. Harmonic approximation was employed to compute the total number and density of vibrational states employing the direct count method,[69] whereas rotational states and hence the dependence of k on J was not taken into account in the present statistical calculations assuming that rotational constants do not change significantly along the path of a unimolecular reaction. Rate constants for various barrierless entrance channels were not computed statistically; instead, the population of different initial complexes produced was assessed through molecular dynamics calculations (*vide infra*). For barrierless exit channels, e.g., H losses leading to **p9-p11**, we utilized the microcanonical variational transition state theory (VTST) approach[71] by considering different positions for the transition state along the reaction path, calculating rate constants corresponding to each of them and finding the minimal rate. Within VTST, we first calculated a series of energies at different distances between two dissociating fragments through partial B2PLYPD3/cc-pVTZ geometry optimization with fixed values of the reaction coordinate. Next, 3N - 7 vibrational frequencies were computed projecting the reaction coordinate out and finally, single-point energies for the optimized structures were refined at the CCSD(T)-F12/cc-pVQZ-f12 level of theory. The RRKM and VTST rate constants were utilized to obtain product branching ratios under single-collision conditions using our inhouse code.[72]

2.2.2. AB INITIO MOLECULAR DYNAMICS SIMULATIONS

The potential energy profile of the title reaction has been identified at the CCSD(T)-F12/cc-pVQZ-f12//B2PLYPD3/cc-pVTZ level of theory (section 2.2.1). However, as millions of energy gradients are needed for ab initio molecular dynamics (AIMD, also known as direct dynamics) simulations in propagating the trajectories, an accurate yet computationally efficient quantum chemistry method must be identified. Therefore, the aforementioned potential energy profile is employed as the benchmark to evaluate the performance of a series of affordable basis sets with B3LYP.[73-75] Previous studies have found that B3LYP is able to identify all intermediates and transition states on the CCSD(T)-F12 PES for similar open shell hydrocarbon system (CH + C_4H_2 and CH + C_4H_6)[76, 77] as well as replicating key features of the product scattering angle and translational energy distributions when used in AIMD. Further, B3LYP has been found to be one of the most effective functionals in minimizing unphysical jumps in total energy over a trajectory. Table S1 in the Supporting Information lists the potential energy profile of this reaction calculated from these various candidate combinations. In this study, further comparison was made with different basis sets before the most accurate, aug-pc-1,[78] was chosen with respect to the benchmark potential energy surface. The minimal root mean square displacement (RMSD) between the benchmark and candidate combination's energies[79] is used to measure the accuracy of the method while the average time per energy gradient calculation (t) is used to measure the efficiency. In general, AIMD seeks to employ the most accurate methods while being affordable, and as a result, B3LYP/aug-pc-1 was selected.

The AIMD simulations are set to model the conditions of the crossed molecular beams experiment. The centers of mass of the reactant molecules, vinylacetylene (C_4H_4) and methylidyne radical (CH), are initially separated by 1000 pm, far enough that the interaction between them is negligible. The relative orientation between these two molecules is randomly sampled. C_4H_4 and CH are set to collide with a fixed relative translational energy of 20.3 kJ mol^{-1}. This translational energy is distributed into both reactant molecules such that the total momentum of the system is zero. The initial vibrational and rotational energies for C_4H_4 are selected from a canonical ensemble at 10 K while the methylidyne radical (CH) is set to be at its ground state. This setting has been shown to accurately model bimolecular collisions in similar conditions.[76, 77, 80] In order to accurately mimicking the conditions of the experiment, the AIMD simulations sample a large ensemble of trajectories. The largest impact parameter, b_{max}, is determined by systematically

increasing the impact parameter b. Starting from b = 0.0 pm with an increment of b_{max} = 100.0 pm, 100 trajectories are sampled at each impact parameter. b_{max} is identified as the largest b where at least one of the trajectories are reactive and further sampling at larger b is deemed as unnecessary due to low reaction probability. Since the trajectories are sampled at discrete b values, the number of trajectories at each impact parameter, $N(b)$, needs to be proportional to its area defined by the ring, $2\pi b\Delta b$.[81] 50 trajectories are sampled at the smallest impact parameter of b_{min} = 100.0 pm and $N(b)$ in this study is computed as:

$$N(b) = N(b_{min}) \cdot \frac{b}{b_{min}}; b \leq b_{max} \quad (1)$$

The positions of atoms are propagated by VENUS (a chemical dynamics software) using the velocity Verlet algorithm with energy gradients calculated using B3LYP/aug-pc-1 in the NWChem quantum chemistry package.[82-84] The AIMD trajectories use a 0.2 fs time step and the conservation of the physical properties (e.g., total energy) of the system is rigorously monitored. Whenever the total energy jumps greater than 4.2 kJ mol^{-1}, the trajectories are restarted. The trajectories are halted once either reactants (i.e., non-reactive collision) or products (i.e., reactive collision) are clearly formed. This occurs when the centers of mass of two groups (A and B) of atoms are separated by more than 10000 pm while a maintaining positive relative velocity ($\overrightarrow{v_{rel}}$) between them, defined as:

$$\overrightarrow{v_{rel}} \cdot \overrightarrow{r_{rel}} > 0 \quad \text{Eq. 2}$$

in which $\overrightarrow{v_{rel}} = \overrightarrow{v_A} - \overrightarrow{v_B}; \overrightarrow{r_{rel}} = \overrightarrow{r_A} - \overrightarrow{r_B}$. $\vec{v}$ and $\vec{r}$ are the center of mass velocity and position of the group of atoms, respectively. A trajectory is also halted once its length has exceeded 8 ps (e.g., 40,000 or more steps) due to the limitation of computational resources and numerical stability, and as demonstrated in section **3.3**, this situation occurs frequently. On average, each 8 ps AIMD trajectory with B3LYP/aug-pc-1 takes 4 days (wall time, ~1.5 hours for initial sampling and ~94.5 hours for trajectory propagation) with 9 Intel Xeon Gold 6342 CPUs (20 cores).

3. RESULTS

3.1. LABORATORY FRAME

For the bimolecular reaction of the methylidyne radical (CH; $X^2\Pi$) with vinylacetylene ($H_2CCHCCH$; X^1A'), reactive scattering signal was observed at mass-to-charge ratios (*m/z*) of 65 ($^{13}CC_4H_4^+$), 64 ($C_5H_4^+$), and 63 ($C_5H_3^+$) with signal at *m/z* = 65 collected at a level of 6 ± 2% with respect to *m/z* = 64. The time-of-flight (TOF) spectra of these *m/z* ratios are identical after scaling (Figure S1); this finding suggests a single reaction channel namely the reaction of the methylidyne radical (CH; 13 amu) with vinylacetylene (C_4H_4; 52 amu) leading to C_5H_4 (64 amu) along with atomic hydrogen (H; 1 amu). The signal at *m/z* = 63 can be associated with dissociative electron impact ionization of the neutral C_5H_4 product in the electron impact ionizer, whereas ion counts at *m/z* = 65 represent the ^{13}C-substituted, ionized molecule $^{13}CC_4H_4^+$ accounting for the natural abundance of ^{13}C. These findings reveal that the C_5H_4 isomer(s) can be prepared through the methylidyne versus atomic hydrogen exchange channel (reaction (R1)). Since ion counts of the parent ion at *m/z* = 64 ($C_5H_4^+$) are collected only at a level of 25 ± 4 % compared to the fragment ion at *m/z* = 63, time-of-flight (TOF) spectra and the full laboratory angular distributions were extracted at the best signal-to-noise ratio of *m/z* = 63 ($C_5H_3^+$). The resulting laboratory angular distribution depicts a distribution maximum at the center-of-mass (CM) angle of 54.0° ± 0.9° and spans at least 38° in the laboratory frame (Figure 1, Table 1). These experimental results suggests that the reaction proceeds through indirect scattering dynamics involving C_5H_5 reaction intermediate(s), which ultimately undergo(es) unimolecular decomposition by ejecting atomic hydrogen to form the neutral C_5H_4 product(s).

Since the atomic hydrogen can be emitted from the methylidyne radical and/or from the vinylacetylene reactant, the reaction of the D1-methylidyne radical (CD; 14 amu) with vinylacetylene (C_4H_4; 52 amu) was conducted as well. TOFs were recorded at *m/z* = 65 ($C_5DH_3^+$) (reaction (R2)) and 64 ($C_5H_4^+/C_5DH_2^+$) (reaction (R3)) at a center-of-mass angle of 52.1º (Figure S2). Here, signal was observed at both *m/z* = 65 and 64 (Figure S2). Ion counts at *m/z* = 64 may also originates from dissociative electron impact ionization of C_5DH_3 if formed through reaction (R2). Accounting for the ^{13}C isotopic contribution of 5.5 % for five carbon atoms, the ratio of the ion counts at *m/z* = 65 versus 64 is calculated to be 30 ± 5%. This data correlates well with the ratio of the ion counts of *m/z* = 64 to *m/z* = 63 in the methylidyne - vinylacetylene system. These findings propose that for the D1-methylidyne - vinylacetylene reaction, ion counts at *m/z* = 64 can

be attributed to a dissociative electron impact ionization of *m/z* = 65 ($C_5DH_3^+$) product(s) in the ionizer, whereas the C_5DH_3 product(s) was (were) formed via *hydrogen atom loss from the vinylacetylene reactant*. In brief, based on the laboratory data alone, we may conclude that, for the reaction of the methylidyne radical (CH; 13 amu) with vinylacetylene ($H_2CCHCCH$; 52 amu), the hydrogen atom loss originates predominantly from the vinylacetylene reactant, but not from the methylidyne radical.

$$CH\ (13\ amu) + C_4H_4\ (52\ amu) \rightarrow C_5H_4\ (64\ amu) + H\ (1\ amu) \quad (R1)$$

$$CD\ (14\ amu) + C_4H_4\ (52\ amu) \rightarrow C_5DH_3\ (65\ amu) + H\ (1\ amu) \quad (R2)$$

$$CD\ (14\ amu) + C_4H_4\ (52\ amu) \rightarrow C_5H_4\ (64\ amu) + D\ (2\ amu) \quad (R3)$$

3.2. CENTER-OF-MASS FRAME

The laboratory data delivered explicit evidence on the gas-phase formation of C_5H_4 isomer(s) under single-collision conditions via atomic hydrogen emission at least from the vinylacetylene reactant. However, the prime directive of our studies is to elucidate the nature of the C_5H_4 isomers formed and to unravel the underlying reaction mechanism(s) on the pertinent C_5H_5 PES accessed via the bimolecular reaction of the methylidyne radical (CH; $X^2\Pi$) with vinylacetylene ($H_2CCHCCH$; X^1A'). To achieve these goals, the laboratory data have to be transformed into the center-of-mass frame[85] by exploiting a forward-convolution routine.[86] This procedure yields the CM translational energy $P(E_T)$ and CM angular $T(\theta)$ flux distributions (Figure 1). Within our error limits, the best-fit CM functions were gained with a single channel fit via reaction (1). The $P(E_T)$ reveals a maximum translational energy release (E_{max}) of 166 ± 26 kJ mol^{-1} for those products formed with minimum internal excitation. Since the maximum translational energy release relates to the reaction energy ($\Delta_r G$) and the collision energy (E_C) via $E_{max} = E_C - \Delta_r G$ due to energy conservation, the reaction is revealed to be exoergic by 146 ± 26 kJ mol^{-1}. Further, the $P(E_T)$ distribution peaks away from zero translational energy at 23 ± 4 kJ mol^{-1}; the average translational energy of the products was derived to be 43 ± 7 kJ mol^{-1} suggesting that only 26 ± 4% of the available energy is released into the translational degrees of freedom of the products. These findings propose indirect scattering dynamics involving C_5H_5 intermediate(s) undergoing unimolecular decomposition through tight exit transition state(s) leading to C_5H_4 molecules from the C_5H_5 intermediates(s).[87, 88] Finally, the $T(\theta)$ depicts a forward−backward symmetry and displays non-zero intensity from 0° to 180°; these findings reveal indirect scattering dynamics through long-

lived C_5H_5 intermediate(s) with lifetimes longer than or at least comparable with their rotation periods.[89]

4. DISCUSSION

4.1. POTENTIAL ENERGY SURFACES (PESs)

The computational investigation of the elementary reaction of the methylidyne radical with vinylacetylene is a daunting task as methylidyne can add to the carbon-carbon double and triple bond as demonstrated in the methylidyne – ethylene [54] and methylidyne – acetylene systems,[90, 91] respectively. Further, methylidyne may insert into carbon-hydrogen single bonds as unraveled in the elementary reaction of methylidyne with dimethylacetylene.[77] Therefore, in the case of polyatomic systems such as the methylidyne – vinylacetylene reaction, it is of great advantage to merge the experimental data with electronic structure calculations and statistical analysis in an attempt to unravel the underlying reaction mechanism(s) (Figures 2-4; Table 2; Figures S3-S6; Table S1-S2). Overall, the addition (C ≡ C, C=C) and insertion pathways along with successive isomerization of the initial reaction intermediates (**i1**, **i2**, **i10**, **i14**, **i22**) involve 33 distinct C_5H_5 intermediates (**i1-i33**) and 67 transition states leading eventually to nine C_5H_4 isomers via emission of atomic hydrogen (**p1-p3**, **p6-p11**). Some of these intermediates can be reasonably expected with chemical intuition, but others are found with the guidance of ab initio molecular dynamics simulation, which will be addressed later in the manuscript. C_5H_4 species include ethynylallene (**p1**; ΔrG = − 230 ± 4 kJ mol^{-1}), 1,4-pentadiyne (**p2**; ΔrG = − 218 ± 4 kJ mol^{-1}), methyldiacetylene (**p3**; ΔrG = − 254 ± 4 kJ mol^{-1}), 1,2,3,4-pentatetraene (**p6**; ΔrG = − 218 ± 4 kJ mol^{-1}), 3-ethynylcyclopropene (**p7**; ΔrG = − 143 ± 4 kJ mol^{-1}), 1-ethynylcyclopropene (**p8**; ΔrG = − 151 ± 4 kJ mol^{-1}), 3-ethenylidenecyclopropene (**p9**; ΔrG = − 122 ± 4 kJ mol^{-1}), 2-ethenylcyclopropene-3-ylidene (**p10**; ΔrG = − 125 ± 4 kJ mol^{-1}), and pent-1-en-4-yne (**p11**; ΔrG = − 77 ± 4 kJ mol^{-1}) with the reaction energies provided in parenthesis. Considering the strain energy of the cyclopropene moiety, **p7-p10** are thermodynamically less stable by up to 100 kJ mol^{-1} compared to the acyclic isomers **p1-p3** and **p6**. Besides the atomic hydrogen loss, the intermediates can also undergo unimolecular decomposition through carbon-carbon bond rupture involving methyl (CH_3) and propargyl radical (C_3H_3) elimination along with diacetylene (C_4H_2; **p4**) and acetylene (C_2H_2; **p5**) (Figures 2-3; Figure S3). Note that in the present experiments, dissociative electron impact ionization of the vinylacetylene reactant produces background counts of CH_3^+, $C_2H_2^+$, $C_3H_3^+$, and

$C_4H_2^+$; therefore, the aforementioned reaction channels involving carbon-carbon bond cleavage cannot be probed under our experimental conditions. A comparison of the experimentally derived reaction energy of 146 ± 26 kJ mol^{-1} with the aforementioned reaction energies energetics suggests that the cyclic isomers 3-ethynylcyclopropene (**p7**), 1-ethynylcyclopropene (**p8**), 3-ethenylidene-cyclopropene (**p9**), 2-ethenylcyclopropene-3-ylidene (**p10**) represent likely products of the elementary reaction of methylidyne with vinylacetylene. The higher energy isomers **p11** might be masked in the low energy section of the CM translational energy distribution P(E_T). For example, if **p11** is solely formed, the resulting translational energy distributions would terminate close to 97 kJ mol^{-1}. This is clearly not observed experimentally. Our electronic structure calculations suggest that the formation of **p7**/**p8** and **p9**/**p10** is initiated by a barrierless addition of the methylidyne radical to the carbon-carbon double and triple bond forming intermediates **i1** and **i10**, respectively (Figures 2 and 3). These cyclic doublet radical intermediates are stabilized by 343 and 368 kJ mol^{-1} with respect to the separated reactants. Unimolecular decomposition of **i1** via atomic hydrogen loss from the C1 and C2 carbon atom can lead to **p7** and **p8**, respectively, via exit transition states located 12 and 21 kJ mol^{-1} above the separated products, respectively. The thermodynamically least stable isomer **p9** is accessible though atomic hydrogen elimination from **i10** after passing a transition state located 6 kJ mol^{-1} above the separated products. The hydrogen migration between the adjacent CH moieties in **i10** yields **i11**. The calculations also reveal that the CH radical may insert into one of the C-H bonds in CH_2 moiety of vinylacetylene forming the chain structure intermediate **i2**, which can isomerize to a cyclic intermediate **i26**. The unimolecular decomposition of **i10**, **i11**, and **i26** leads to the product **p10**. In this sense, the formation of **p7**/**p8** and **p9**/**p10** involves indirect scattering dynamics through three-membered ring, doublet C_5H_5 collision complexes via a de-facto methylidyne addition – atomic hydrogen elimination pathway involving tight (**p7**/**p8**/**p9**) and loose (**p10**) exit transition states. The indirect scattering dynamics (through long lived C_5H_5 reaction intermediates) along with the presence of a tight exit transition state (**p7**/**p8**/**p9**) was contemplated from the experimental findings (3.1 and 3.2), whereas the formation of **p10** via a loose exit transition state reveals the discrepancy with the experimental results. Therefore, **p10** can be eliminated as a predominant product. Further, the experimental data from the D1-methylidyne – vinylacetylene system revealed that the ejected hydrogen atom originates predominantly from the vinylacetylene reactant, which is in agreement with the computationally predicted reaction mechanism (Figures S4-S6). For the initial intermediate **i1** (Figure 3), the

decomposition behaviors of **i1** → **p7**/**p8** with significant barriers of over 213 kJ mol^{-1} are less competitive than the isomerization process **i1** → **i2** with barrier of only 73 kJ mol^{-1}. In contrast with intermediate **i1**, the decomposition process **i10** → **p9** carries lowest barrier compared with the isomerization pathways **i10** → **i11**/**i12**/**i13**. Therefore, the formation of products **p7** and **p8** can be ruled out. These findings suggest that **p9** is the likely product.

Under 'normal' circumstances, the formation of lower energy products **p1**, **p2**, **p3**, and **p6** with overall reaction energies of -218 ± 4 to -254 ± 4 kJ mol^{-1} can be excluded considering the discrepancy between the theoretically predicted and experimentally derived reaction energy of -146 ± 26 kJ mol^{-1}. However, recent crossed molecular beam studies suggested that in the case of polyatomic reactions, the nascent reaction products can be highly rovibrationally excited thus shifting the high energy cutoff of the center-of-mass translational energy distribution to energies lower than the reaction energies computed for products in the rotational and vibrational ground states.[77] This might be also the case for **p1**, **p2**, **p3**, and **p6**. Based on the computed surfaces, the initial addition complexes **i1** and **i10** along with the insertion intermediates **i2**, and **i14** may undergo extensive isomerization involving ring openings and hydrogen migrations to eventually yield **p1**, **p2**, **p3**, and **p6** via tight exit transition states.

Isotopic substitution experiments can provide further clarification. The potential energy surface of the D1-methylidyne – vinylacetylene system (Figures S4 and S5) allows tracing the extent to which the reaction intermediates lose atomic hydrogen versus atomic deuterium. If **p1** or **p3** is formed via initial intermediate **i10** or **i14**, both the atomic deuterium *and* hydrogen loss should be observable. Within our error limits this is not observed. If **p1**, **p2**, and **p3** are formed via initial intermediate **i1** or **i2**, whereas **p6** originated from initial intermediate **i10** or **i14**, only hydrogen atom loss should be detected, which can match our isotopic substitution experimental results. The products **p1**, **p2**, **p3**, and **p6** can be narrowed down even further. Compared with the product **p1**, the pathways lead to the formation of **p2** and **p3** involve higher barriers and more isomerization steps. Therefore, the product **p1** would be the dominant product via initial intermediate **i2**, with **p2** and **p3** being minor products. The product **p6** may be the dominant product via intermediate **i14**, as the product **p9** is the dominant product via intermediate **i10**. Hence, we may conclude that **p2** or **p3** do not represent the dominating reaction products. However, in case of **p1** and **p6** only the

atomic hydrogen loss is predicted, and therefore these isomers could be formed highly rovibrationally excited thus resulting in a center-of-mass translational energy distribution shifted toward lower energies than the computed reaction energies. In brief, a comparison of the experimental data with electronic structure calculations proposes that based on energy conservation, the cyclic isomer 3-ethenylidenecyclopropene (**p9**) is formed via the pathway **i10** → **p9**. However, if the products are formed with extensive rovibrational excitation, this internal energy along with the results from isotopic substitution experiments may also account for the formation of the acyclic isomers ethynylallene (**p1**) via the pathways **i3**/**i4**/**i5** → **p1** and/or 1,2,3,4-pentatetraene (**p6**) through **i14** → **p6**. Recall that, the distribution minimum of *T(θ)* at 90° proposes geometrical limitations and an emission of hydrogen atom nearly perpendicularly to the total angular momentum vector nearly within the rotational plane of the fragmenting complex(es). The computed geometries of the exit transition states lead to **p1** via **i3**/**i5** → **p1** (Figure 5) with the hydrogen atom ejected both at angles of 0°. This in-plane emission matches the experimental prediction of the ejection direction of the hydrogen atom based on the *T(θ)*.[85, 89] However, the transition states for **i4** → **p1**, **i14** → **p6**, **i10** → **p9** with the hydrogen atom ejected at angles of 71°, 90°, and 90° (Figure 5), can account for the sideways scattering.[85, 89] Therefore, **p6** and **p9** can be eliminated as predominant products. In conclusion, **p1** is the most likely products formed under our experimental conditions via **i3**/**i5** → **p1**. These exoergicities (**p1**; $\Delta rG = -230 \pm 4$ kJ mol^{-1}) do not correlate with our experimentally determined reaction energy of -146 ± 26 kJ mol^{-1}. This could mean that the reaction is statistically leading to **p1**, but a significant amount of available energy is channeled into internal excitation of the polyatomic reaction products. This would in turn lead to a shift of the maximum energy release to values significantly lower than in the limit of zero internal excitation.

4.2. STATISTICAL CALCULATIONS

We also utilized Rice−Ramsperger−Kassel−Marcus (RRKM)[92] theory to predict the branching ratios of the C_5H_4 isomers formed within the limit of a complete energy randomization of the initial collision complexes resulting from addition to the carbon-carbon double (**i1**) and triple bonds (**i10**) along with the methylidyne insertion intermediates into the CH and methylenic (CH_2) moieties (**i14**, **i22**, **i2**) under zero-pressure conditions. These conditions correspond to a crossed

molecular beams experiment, where a single collision between the reactants is followed by unimolecular decomposition of initial complexes without a possibility of any collisional energy transfer. The initial population was derived from quasiclassical trajectory (QCT) simulations, which are combined with RRKM calculations for five distinct scenarios where *only* **i1, i2**, **i10**, **i14**, or **i22** are formed in the entrance channel (Table 2). In the limit of complete energy randomization, the additions to the carbon-carbon double and triple bonds predicts predominantly lead to the formation of ethynylallene (**p1**) at levels of nearly 90 %. Whereas for the double-bond addition forming **i1** the pathway to this product is straightforward, **i1** $\rightarrow$ **i2** $\rightarrow$ **i3** $\rightarrow$ **p1** + H, the triple-bond addition complex **i10** first undergoes a 1,2-H shift in its three-membered ring accompanied by the ring opening leading to a metastable species **i33**, which is then subjected to a spontaneous H migration forming **i2** and the latter dissociates to **p1** via **i3**. Further, RRKM predicts that the insertion pathways, may lead eventually to ethynylallene (**p1**) through **i2**, 1,2,3,4-pentatetraene (**p6**) via **i14**, and 1,4-pentadiyne (**p2**) via **i22** at levels of 90%, 54%, and 68%, respectively. Recall that 1,4-pentadiyne (**p2**) and 1,2,3,4-pentatetraene (**p6**) are eliminated as major contributors to the reactive scattering signal due to isotopic substitution experiments and the distribution minimum of $T(\theta)$ at 90°. Overall, RRKM calculations predict that the hitherto elusive ethynylallene (**p1**) represent dominant reaction product – based on our experimental data - highly rovibrationally excited if the methylidyne radical inserts into the methylenic (CH_2) carbon-hydrogen bond (**i2**) and/or adds to the double (**i1**) or triple carbon-carbon bond (**i10**). Hence, we may conclude at least qualitatively that ethynylallene (**p1**) represents the dominating reaction product. However, ab initio molecular dynamics (AIMD) simulations are imperative to validate these suggestions.

4.3. AB INITIO MOLECULAR DYNAMICS SIMULATIONS

In *ab initio* molecular dynamics (AIMD, also known as direct dynamics),[82] the motion of atoms is propagated interactively according to the forces (i.e., energy gradients) computed by quantum chemistry methods. Compared to statistical theories that based on a static potential energy profile (e.g., RRKM), AIMD does not rely on the presumptions made in deriving such theories and can capture the non-equilibrium, non-statistical nature of the reaction. In addition, properties such as scattering angles and relative translational energy distributions of the products can be directly measured and compared with experiments.

Of the 750 trajectories in which methylidyne radical (CH; $X^2\Pi$) and vinylacetylene ($H_2CCHCCH$; X^1A') collide at different impact parameters, 14.9 % reacted (i.e., forming some intermediates after the collision) and the rest are non-reactive collisions. Of the reactive trajectories, only 6.3% ultimately dissociated to form product within 8 ps (40,000 or more steps, section **2.2.2**), while the other 93.7 % formed long life-time intermediates and frequent isomerization was observed. This result is very surprising – AIMD simulations of bimolecular collisions of systems of similar potential energy profiles and excitations (e.g., collision energy, vibrational and rotational states), methylidyne radical (CH; $X^2\Pi$) with dimethylacetylene (CH_3CCCH_3; X^1A')[76] and methylidyne radical with diacetylene (HCCCCH; $X\ ^1A'$),[77] demonstrated a much larger ratio (44% and 100%, respectively) of forming product with the same amount of simulation. Among these 6.3 % reactive trajectories that form products, only 25% undergoes direct reaction. The reactive trajectories form **p10** and **p11** with a ratio of 1:1. Both the lack of direct reactions and the long-lived intermediates found in AIMD support the experimental conjecture that the methylidyne radical (CH; $X^2\Pi$) and vinylacetylene ($H_2CCHCCH$; X^1A') collision predominantly goes through indirect reactions.

As argued in section **2.2.2.**, extending 750 AIMD trajectories beyond 8 ps exceeds the capacity of the computational resources available to us. Nonetheless, those AIMD trajectories trapped at various intermediates are still valuable to predict the product branching ratio – the average time that it takes for the methylidyne radical (CH; $X^2\Pi$) and vinylacetylene ($H_2CCHCCH$; X^1A') to collide is only ~0.4 ps – because the lifetime of the intermediates (~7.6 ps) is much longer than the intramolecular vibrational energy redistribution (IVR) which is typically less than 1 ps.[93] Under such conditions, all vibrational modes of the intermediate can be assumed to have equilibrated. Therefore, the AIMD-correct RRKM product branching ratios are estimated as the weighted average of the RRKM product branching ratios from each intermediate resulting from the collision between methylidyne radical (CH; $X^2\Pi$) and vinylacetylene ($H_2CCHCCH$; X^1A'), of which the weights are the populations of intermediates determined from AIMD trajectories.

The AIMD trajectories are examined by comparing the dynamic molecular graph against that of the intermediates and products. In molecular graph, edges (bonds) exist between nodes (atoms) *i* and *j* of the graph if $r_{ij} < 300$ pm and each hydrogen has at most one edge, which is to the atom closest to it. Each intermediate on the potential energy profile (Figures 2-4 and Figure S3) in principle has a unique molecular graph. During a trajectory, a certain intermediate is considered

to have formed if it has an isomorphic molecular graph to the current frame. Most trajectories form **i1** *immediately* after collision, followed by **i2**/**i3**, but quickly, the three-membered ring in **i1** breaks and **i2**/**i3** becomes the majority after just 0.1 ps until the end of the simulation (e.g., 8 ps). At this point, virtually all **i1** has been depleted, although minor concentrations of **i22** and **i14** are present. Additionally, a minor amount of **i10** formed immediately after the collision but slowly depletes to zero. The population of various intermediates after the collision is shown in Figure 6. Animations of representative trajectories are provided in the Supporting Information.

These populations of the intermediates by the end of the AIMD simulation are used as the weights in the AIMD-corrected product branching ratio, which results in 75.2 % **p1**, 10.0 % **p2**, 4.6% **p3**, 1.4% **p4**, 3.8% **p5**, 2.0 % **p6**, 0.2% **p7**, 0.1% **p8**, and 2.7 % **p9**. The results can match the experimental and RRKM determined potential product **p1**. A possible factor that could contribute to this agreement is that the product molecules are highly rovibrational excited, as mediated by the long lifetime of the intermediates and sufficient IVR, which makes the detection of product molecules with large translational energy unlikely. This effect would shift the time-of-flight distribution (Figure 1) toward smaller values. A similar phenomenon was reported in the reaction of methylidyne plus dimethylacetylene (C_4H_6).

5. CONCLUSIONS

Our crossed molecular beams experiment on the reaction of the methylidyne (CH; $X^2\Pi$) radical with vinylacetylene ($H_2CCHCCH$; X^1A') reveals that it proceeds barrierlessly via indirect scattering dynamics through long-lived C_5H_5 reaction intermediate(s) ultimately dissociating to C_5H_4 isomers along with atomic hydrogen. Isotopic substitution experiments were also performed by replacing the methylidyne (CH) radical with D1-methylidyne, which revealed that the atomic hydrogen is lost predominantly from the vinylacetylene reactant in the methylidyne – dimethylacetylene reaction. The center of mass functions suggest an overall reaction energy of -146 ± 26 kJ mol^{-1} with the CM angular distribution $T(\theta)$ depicts a forward−backward symmetry and displays non-zero intensity from 0° to 180°; these findings reveal indirect scattering dynamics through long-lived C_5H_5 intermediate(s) with lifetimes longer than or at least comparable with their rotation periods. Ab initio electronic structure and statistical RRKM calculations, suggests that **p1** (**i1**/**i2**/**i10**), **p6** (**i14**), and **p2** (**i22**) with the initial complexes provided in parenthesis are the most likely atomic hydrogen loss products. The reaction has no entrance barrier; all barriers

involved in the formation of **p1**, **p6**, and **p2** are well below the energy of the separated reactants, and the overall reactions to prepare the three isomers are exoergic by -230 ± 4 kJ mol^{-1} (**p1**), -218 ± 4 kJ mol^{-1} (**p6**), and -218 ± 4 kJ mol^{-1} (**p2**), respectively. These energies do not match the experimentally derived reaction energy of -146 ± 26 kJ mol^{-1}. If **p1**, **p6**, and **p2** are also formed, suggesting that the reaction is either non-statistical or that a significant amount of the energy is channeled into the internal rovibrational modes of the heavy products. However, the products **p6** and **p2** may be ruled out based on the distribution minimum of $T(\theta)$ at 90° and isotopic substitution experiments, respectively, whereas the formation mechanisms of **p1** can match the experimental findings well. AIMD simulations were also performed and revealed that the reaction dynamics leading predominantly to **p1** (75.2 %) and minor products are **p2**, **p3**, **p6**, **p9** (19.3 %). The dominating pathways reveal an addition of methylidyne to the carbon-carbon double bond of vinylacetylene leading to the cyclic intermediate **i1**, followed by **i2**/**i3**; however, the three-membered ring in **i1** breaks quickly and **i2**/**i3** becomes the majority. The intermediates **i10**, **i14**, and **i22** carry minor contributions. These finding propose that the combination of the crossed molecular beam experiments with electronic structure calculations and quasiclassical trajectory (QCT) studies provide persuasive evidence on the formation of ethynylallene (**p1**) under single collision conditions via the bimolecular reaction of the methylidyne radical with vinylacetylene in the gas phase involving indirect scattering dynamics.

SUPPORTING INFORMATION

Computational details, optimized cartesian coordinates and vibrational frequencies for all intermediates, transition states, reactants and products involved in the reactions of the methylidyne radical with vinylacetylene, additional figures and tables are included.

Acknowledgements

This work was supported by the U.S. Department of Energy, Basic Energy Sciences under grants DE-FG02-03ER15411 and DE-FG02-04ER15570 to the University of Hawaii and to Florida International University, respectively. This work is also supported by the National Science Foundation under Grant No. 2144031. The authors appreciate the information technology service (ITS) from the University of Hawai'i, Manoa for the computational resources.

Conflict of interest

The authors declare no conflict of interest.

References:

1. H. Richter and J. B. Howard, *Prog. Energy Combust. Sci.*, 2000, **26**, 565-608.
2. W. W. Duley, *Faraday Discuss.*, 2006, **133**, 415-425.
3. M. Frenklach and E. D. Feigelson, *Astrophys. J.*, 1989, **341**, 372-384.
4. A. G. G. M. Tielens, *Annu. Rev. Astron. Astrophys.*, 2008, **46**, 289-337.
5. N. A. Eaves, S. B. Dworkin and M. J. Thomson, *Proc. Combust. Inst.*, 2017, **36**, 935-945.
6. Z. A. Mansurov, *Combust. Explos. Shock Waves*, 2005, **41**, 727-744.
7. K.-H. Kim, S. A. Jahan, E. Kabir and R. J. C. Brown, *Environ. Int.*, 2013, **60**, 71-80.
8. D. Majumdar, B. Rajaram, S. Meshram and C. V. Chalapati Rao, *Crit. Rev. Env. Sci. Technol.*, 2012, **42**, 1191-1232.
9. B. M. Jones, F. Zhang, R. I. Kaiser, A. Jamal, A. M. Mebel, M. A. Cordiner and S. B. Charnley, *Proc. Natl. Acad. Sci. U.S.A*, 2011, **108**, 452-457.
10. N. Balucani, O. Asvany, Y. Osamura, L. C. L. Huang, Y. T. Lee and R. I. Kaiser, *Planet. Space Sci.*, 2000, **48**, 447-462.
11. H. Naraoka, A. Shimoyama and K. Harada, *Earth and Planetary Science Letters*, 2000, **184**, 1-7.
12. L. Becker and T. E. Bunch, *Meteorit. Planet. Sci.*, 1997, **32**, 479-487.
13. M. P. Callahan, A. Abo-Riziq, B. Crews, L. Grace and M. S. de Vries, *Spectrochim. Acta, Part A*, 2008, **71**, 1492-1495.
14. L. d'Hendecourt and P. Ehrenfreund, *Adv. Space Res.*, 1997, **19**, 1023-1032.
15. E. F. van Dishoeck, *Publ. Astron. Soc. Pac.*, 2000, **112**, 286.
16. Y. M. Rhee, T. J. Lee, M. S. Gudipati, L. J. Allamandola and M. Head-Gordon, *Proc. Natl. Acad. Sci. U.S.A*, 2007, **104**, 5274-5278.

17. L. J. Allamandola, A. G. G. M. Tielens and J. R. Barker, *Astrophys. J. Suppl. Ser.*, 1989, **71**, 733-775.
18. M. Steglich, J. Bouwman, F. Huisken and T. Henning, *Astrophys. J.*, 2011, **742**, 2.
19. M. Steglich, C. Jäger, G. Rouillé, F. Huisken, H. Mutschke and T. Henning, *Astrophys. J.*, 2010, **712**, L16.
20. A. M. Ricks, G. E. Douberly and M. A. Duncan, *Astrophys. J.*, 2009, **702**, 301.
21. P. Schmitt-Kopplin, Z. Gabelica, R. D. Gougeon, A. Fekete, B. Kanawati, M. Harir, I. Gebefuegi, G. Eckel and N. Hertkorn, *Proc. Natl. Acad. Sci. U.S.A*, 2010, **107**, 2763-2768.
22. L. M. Ziurys, *Proc. Natl. Acad. Sci. U.S.A*, 2006, **103**, 12274-12279.
23. M. P. Bernstein, S. A. Sandford, L. J. Allamandola, J. S. Gillette, S. J. Clemett and R. N. Zare, *science*, 1999, **283**, 1135-1138.
24. P. Ehrenfreund and M. A. Sephton, *Faraday Discuss.*, 2006, **133**, 277-288.
25. E. Herbst and E. F. van Dishoeck, *Annu. Rev. Astron. Astrophys.*, 2009, **47**, 427-480.
26. A. M. Mebel, V. V. Kislov and R. I. Kaiser, *J. Am. Chem. Soc.*, 2008, **130**, 13618-13629.
27. S. Messenger, S. Amari, X. Gao, R. M. Walker, S. J. Clemett, X. D. F. Chillier, R. N. Zare and R. S. Lewis, *Astrophys. J.*, 1998, **502**, 284.
28. S. Mostefaoui, P. Hoppe and A. El Goresy, *Science*, 1998, **280**, 1418-1420.
29. P. P. K. Smith and P. R. Buseck, 1982.
30. W. W. Duley, *Astrophys. J.*, 2000, **528**, 841.
31. S. Amari, R. S. Lewis and E. Anders, *Geochimica et Cosmochimica Acta*, 1995, **59**, 1411-1426.
32. E. Zinner, S. Amari, B. Wopenka and R. S. Lewis, *Meteoritics*, 1995, **30**, 209-226.
33. J. Cami, J. Bernard-Salas, E. Peeters and S. E. Malek, *Science*, 2010, **329**, 1180-1182.
34. A. L. Lafleur, J. B. Howard, J. A. Marr and T. Yadav, *J. Phys. Chem.*, 1993, **97**, 13539-13543.
35. N. S. Goroff, *Acc. Chem. Res.*, 1996, **29**, 77-83.
36. A. L. Lafleur, J. B. Howard, K. Taghizadeh, E. F. Plummer, L. T. Scott, A. Necula and K. C. Swallow, *J. Phys. Chem.*, 1996, **100**, 17421-17428.
37. L. Vereecken, J. Peeters, H. F. Bettinger, R. I. Kaiser, P. v. R. Schleyer and H. F. Schaefer, *J. Am. Chem. Soc.*, 2002, **124**, 2781-2789.
38. A. Raj, I. D. C. Prada, A. A. Amer and S. H. Chung, *Combust. Flame*, 2012, **159**, 500-515.
39. S. Park, Y. Wang, S. H. Chung and S. M. Sarathy, *Combust. Flame*, 2017, **178**, 46-60.
40. A. D'Anna and A. Violi, *Energy & fuels*, 2005, **19**, 79-86.
41. M. S. Skjøth-Rasmussen, P. Glarborg, M. Østberg, J. T. Johannessen, H. Livbjerg, A. D. Jensen and T. S. Christensen, *Combust. Flame*, 2004, **136**, 91-128.
42. N. l. Kunioshi, M. Touda and S. Fukutani, *Combust. Flame*, 2002, **128**, 292-300.
43. P. Lindstedt, L. Maurice and M. Meyer, *Faraday Discuss.*, 2002, **119**, 409-432.
44. G. Da Silva, *J. Phys. Chem. A*, 2017, **121**, 2086-2095.
45. F. Stahl, P. von Ragué Schleyer, H. F. Bettinger, R. I. Kaiser, Y. T. Lee and H. F. Schaefer III, *J. Chem. Phys.*, 2001, **114**, 3476-3487.
46. R. I. Kaiser, C. C. Chiong, O. Asvany, Y. T. Lee, F. Stahl, P. von R. Schleyer and H. F. Schaefer III, *J. Chem. Phys.*, 2001, **114**, 3488-3496.
47. F. Zhang, S. Kim and R. I. Kaiser, *Phys. Chem. Chem. Phys.*, 2009, **11**, 4707-4714.
48. F. Stahl, P. v. R. Schleyer, H. F. Schaefer III and R. I. Kaiser, *Planet. Space Sci.*, 2002, **50**, 685-692.
49. A. Jamal and A. M. Mebel, *Phys. Chem. Chem. Phys.*, 2010, **12**, 2606-2618.
50. R. I. Kaiser, Y. T. Lee and A. G. Suits, *J. Chem. Phys.*, 1995, **103**, 10395-10398.
51. R. Kaiser, A. M. Mebel and Y. T. Lee, *J. Chem. Phys.*, 2001, **114**, 231-239.
52. R. I. Kaiser, P. Maksyutenko, C. Ennis, F. Zhang, X. Gu, S. P. Krishtal, A. M. Mebel, O. Kostko and M. Ahmed, *Faraday Discuss.*, 2010, **147**, 429-478.
53. A. M. Thomas, L. Zhao, C. He, G. R. Galimova, A. M. Mebel and R. I. Kaiser, *Angew. Chem. Int. Ed.*, 2019, **58**, 15488-15495.

54. F. Zhang, P. Maksyutenko and R. I. Kaiser, *Phys. Chem. Chem. Phys.*, 2012, **14**, 529-537.
55. E. Tørneng, C. J. Nielsen, P. Klaeboe, H. Hopf and H. Priebe, *Spectrochim. Acta, Part A*, 1980, **36**, 975-987.
56. G. O. Brink, *Rev. Sci. Instrum.*, 1966, **37**, 857-860.
57. N. R. Daly, *Rev. Sci. Instrum.*, 1960, **31**, 264-267.
58. P. S. Weiss, Ph. D. Dissertation Thesis, University of California, 1986.
59. M. F. Vernon, Ph. D. Dissertation Thesis, University of California, 1983.
60. S. Grimme, S. Ehrlich and L. Goerigk, *J. Comput. Chem.*, 2011, **32**, 1456-1465.
61. L. Goerigk and S. Grimme, *J. Chem. Theory Comput.*, 2011, **7**, 291-309.
62. S. Grimme, *J. Chem. Phys.*, 2006, **124**, 034108.
63. T. H. Dunning, *J. Chem. Phys.*, 1989, **90**, 1007-1023.
64. T. B. Adler, G. Knizia and H.-J. Werner, *J. Chem. Phys.*, 2007, **127**, 221106.
65. G. Knizia, T. B. Adler and H.-J. Werner, *J. Chem. Phys.*, 2009, **130**, 054104.
66. J. Zhang and E. F. Valeev, *J. Chem. Theory Comput.*, 2012, **8**, 3175-3186.
67. M. J. Frisch, G. W. Trucks, H. B. Schlegel, G. E. Scuseria, M. A. Robb, J. R. Cheeseman, G. Scalmani, V. Barone, B. Mennucci, G. A. Petersson, H. Nakatsuji, M. Caricato, X. Li, H. P. Hratchian, A. F. Izmaylov, J. Bloino, G. Zheng, J. L. Sonnenberg, M. Hada, M. Ehara, K. Toyota, R. Fukuda, J. Hasegawa, M. Ishida, T. Nakajima, Y. Honda, O. Kitao, H. Nakai, T. Vreven, J. A. Montgomery, Jr., J. E. Peralta, F. Ogliaro, M. Bearpark, J. J. Heyd, E. Brothers, K. N. Kudin, V. N. Staroverov, R. Kobayashi, J. Normand, K. Raghavachari, A. Rendell, J. C. Burant, S. S. Iyengar, J. Tomasi, M. Cossi, N. Rega, J. M. Millam, M. Klene, J. E. Knox, J. B. Cross, V. Bakken, C. Adamo, J. Jaramillo, R. Gomperts, R. E. Stratmann, O. Yazyev, A. J. Austin, R. Cammi, C. Pomelli, J. W. Ochterski, R. L. Martin, K. Morokuma, V. G. Zakrzewski, G. A. Voth, P. Salvador, J. J. Dannenberg, S. Dapprich, A. D. Daniels, Ö. Farkas, J. B. Foresman, J. V. Ortiz, J. Cioslowski and D. J. Fox, *Gaussian 16, Revision B.01*, Gaussian, Inc. Wallingford, CT, 2016.
68. H.-J. Werner, P. J. Knowles, G. Knizia, F. R. Manby, M. Schütz, P. Celani, W. Györffy, D. Kats, T. Korona, R. Lindh, A. Mitrushenkov, G. Rauhut, K. R. Shamasundar, T. B. Adler, R. D. Amos, A. Bernhardsson, A. Berning, D. L. Cooper, J. O. Deegan, A. J. Dobbyn, F. Eckert, E. Goll, C. Hampel, A. Hesselmann, G. Hetzer, T. Hrenar, G. Jansen, C. Köppl, Y. Liu, A. W. Lloyd, R. A. Mata, A. J. May, S. J. McNicholas, W. Meyer, M. E. Mura, A. Nicklass, D. P. O'Neill, P. Palmieri, D. Peng, K. Pflüger, R. Pitzer, M. Reiher, T. Shiozaki, H. Stoll, A. J. Stone, R. Tarroni, T. Thorsteinsson and M. Wang, *MOLPRO, Version 2021, A Package of Ab Initio Programs*, University of Cardiff, Cardiff, UK, 2021; http://www.molpro.net.
69. H. Eyring, S. H. Lin and S. M. Lin, *Basic chemical kinetics*, John Wiley and Sons, Inc., New York, 1980.
70. V. V. Kislov, T. L. Nguyen, A. M. Mebel, S. H. Lin and S. C. Smith, *J. Chem. Phys.*, 2004, **120**, 7008-7017.
71. J. I. Steinfeld, J. S. Francisco and W. L. Hase, *Chemical Kinetics and Dynamics*, Prentice Hall Upper Saddle River, New Jersey, 1999.
72. C. He, L. Zhao, A. M. Thomas, A. N. Morozov, A. M. Mebel and R. I. Kaiser, *J. Phys. Chem. A*, 2019, **123**, 5446-5462.
73. A. D. Becke, *J. Chem. Phys.*, 1993, **98**, 1372-1377.
74. C. Lee, W. Yang and R. G. Parr, *Phys. Rev. B*, 1988, **37**, 785-789.
75. A. D. Becke, *J. Chem. Phys.*, 1992, **98**, 5648.
76. C. He, G. R. Galimova, Y. Luo, L. Zhao, A. K. Eckhardt, R. Sun, A. M. Mebel and R. I. Kaiser, *Proc. Natl. Acad. Sci. U.S.A*, 2020, **117**, 30142-30150.
77. C. He, K. Fujioka, A. A. Nikolayev, L. Zhao, S. Doddipatla, V. N. Azyazov, A. M. Mebel, R. Sun and R. I. Kaiser, *Phys. Chem. Chem. Phys.*, 2022, DOI: https://doi.org/10.1039/D1CP04443E.

78. F. Jensen, *J. Chem. Phys.*, 2001, **115**, 9113-9125.
79. K. Fujioka, K.-M. Weitzel and R. Sun, *J. Phys. Chem. A*, 2022, **126**, 1465-1474.
80. S. Doddipatla, C. He, R. I. Kaiser, Y. Luo, R. Sun, G. R. Galimova, A. M. Mebel and T. J. Millar, *Proc. Natl. Acad. Sci. U.S.A*, 2020, **117**, 22712-22719.
81. Y. Luo, K. Fujioka, A. Shoji, W. L. Hase, K.-M. Weitzel and R. Sun, *J. Phys. Chem. A*, 2020, **124**, 9119-9127.
82. M. Paranjothy, R. Sun, Y. Zhuang and W. L. Hase, *Wiley Interdisciplinary Reviews: Computational Molecular Science*, 2013, **3**, 296-316.
83. X. Hu, W. L. Hase and T. Pirraglia, *J. Comput. Chem.*, 1991, **12**, 1014-1024.
84. M. Valiev, E. J. Bylaska, N. Govind, K. Kowalski, T. P. Straatsma, H. J. J. Van Dam, D. Wang, J. Nieplocha, E. Apra, T. L. Windus and W. A. de Jong, *Comput. Phys. Commun.*, 2010, **181**, 1477-1489.
85. R. I. Kaiser, Y. T. Lee and A. G. Suits, *J. Chem. Phys.*, 1996, **105**, 8705-8720.
86. R. I. Kaiser, D. Stranges, Y. T. Lee and A. G. Suits, *J. Chem. Phys.*, 1996, **105**, 8721-8733.
87. R. D. Levine, *Molecular Reaction Dynamics*, Cambridge University Press, Cambridge, 2005.
88. D. R. Herschbach, *Discuss. Faraday Soc.*, 1962, **33**, 149-161.
89. W. B. Miller, S. A. Safron and D. R. Herschbach, *Discuss. Faraday Soc.*, 1967, **44**, 108-122.
90. R. I. Kaiser, X. Gu, F. Zhang and P. Maksyutenko, *Phys. Chem. Chem. Phys.*, 2012, **14**, 575-588.
91. P. Maksyutenko, F. Zhang, X. Gu and R. I. Kaiser, *Phys. Chem. Chem. Phys.*, 2011, **13**, 240-252.
92. J. I. Steinfeld, J. S. Francisco and W. L. Hase, *Chemical Kinetics and Dynamics*, Prentice Hall, Englewood Cliffs, New Jersey, 1982.
93. T. Baer and W. L. Hase, *Unimolecular Reaction Dynamics (International Series of Monographs on Chemistry)*, Oxford University Press, New York, 1996.

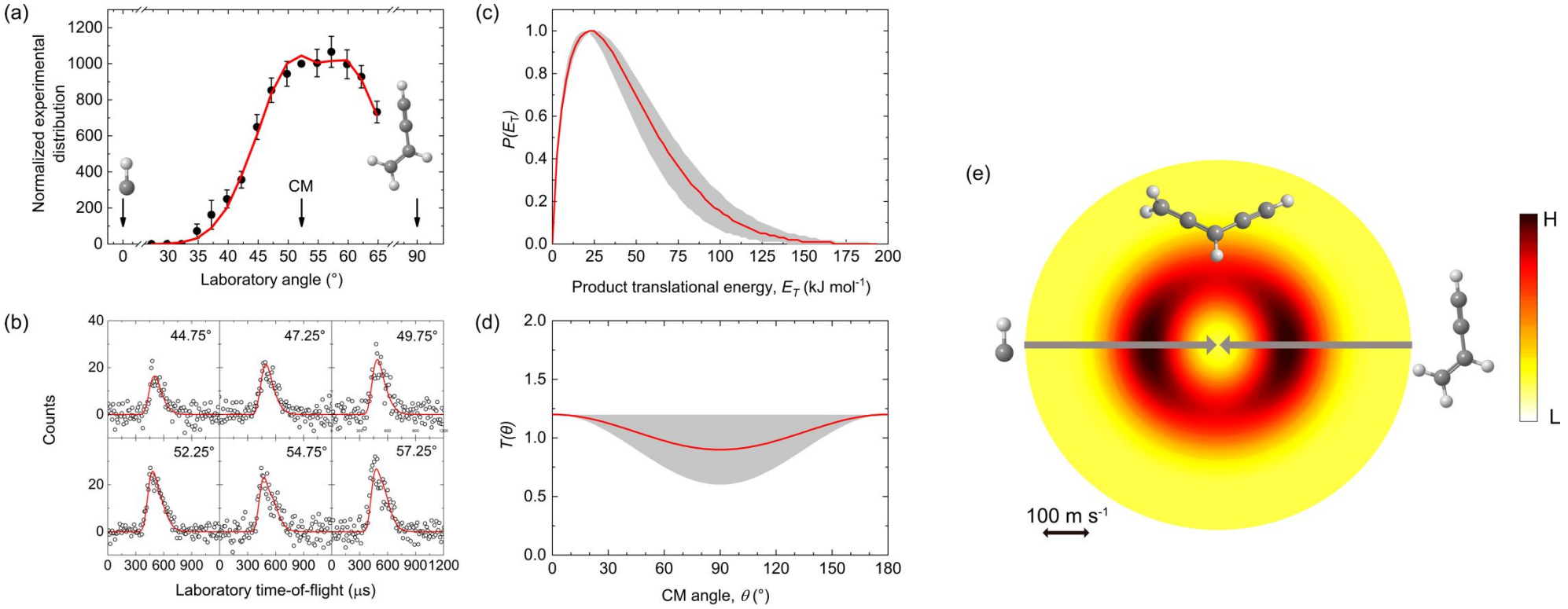

Figure 1. Laboratory angular distributions of the products recorded at m/z = 63 ($C_5H_3^+$) for the reaction of the methylidyne radical with vinylacetylene (a). The solid circles represent the experimental data, CM designates the center-of-mass angle, the error bars represent the 1 σ standard deviation and red solid lines represent the overall fit. Selected TOF spectra are presented in panel (b); open circles depict the experimental data and the solid lines the fit. Center-of-Mass (CM) translational energy distribution $P(E_T)$ (c) and angular distribution $T(\theta)$ (d) along with the associated flux contour map (e) leading to the formation of ethynylallene (**p1**). Shaded areas indicate the error limits of the best fits accounting for the uncertainties of the laboratory angular distribution and TOF spectra, with the red solid lines defining the best-fit functions. The flux contour map represents the flux intensity of the reactive scattering products as a function of the CM scattering angle (θ) and product velocity (u). The color bar indicates the flux gradient from high (H) intensity to low (L) intensity. Atoms are color coded as follows: carbon (black), and hydrogen (grey).

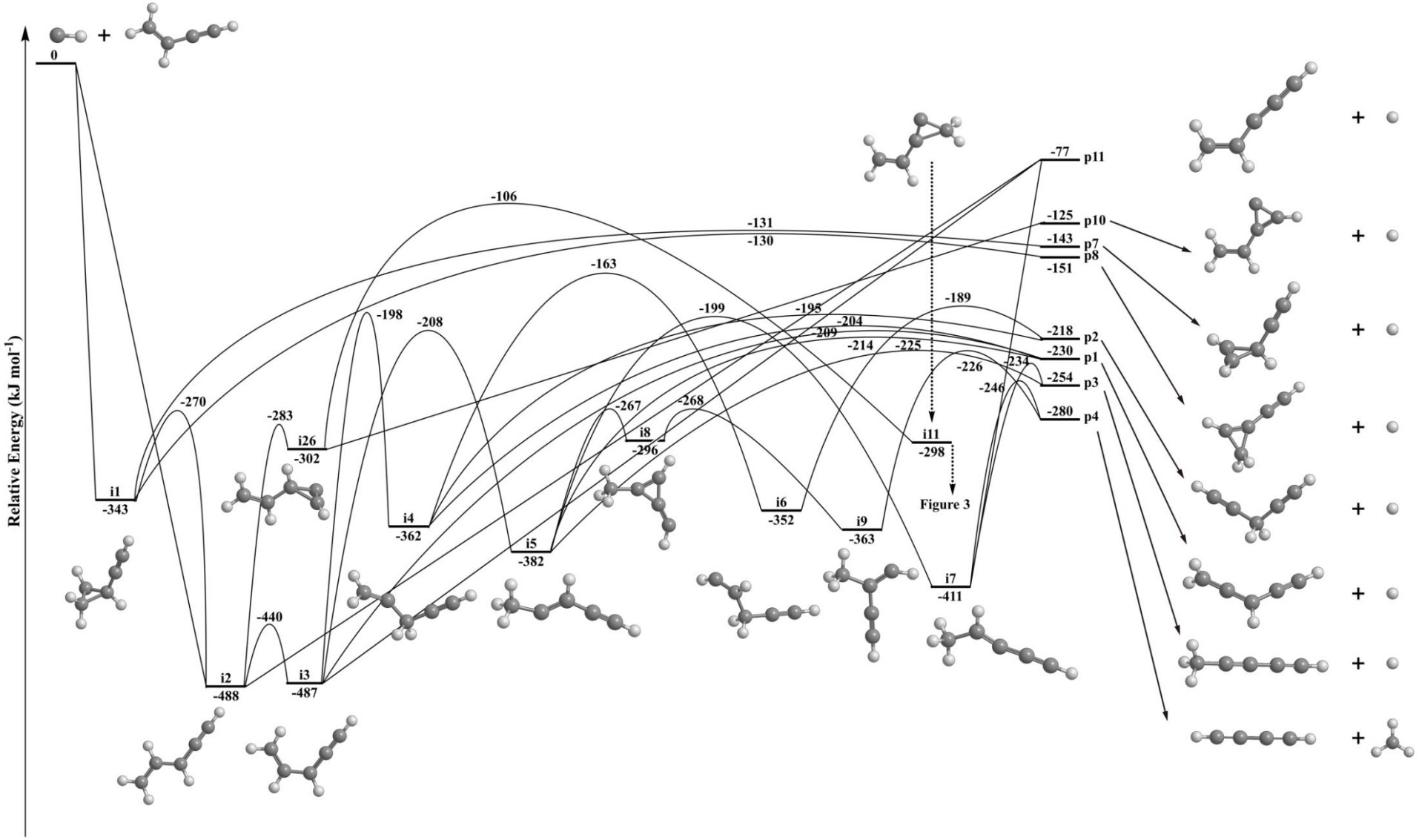

Figure 2. Schematic representation of the portion of C_5H_5 potential energy surface (PES) leading to **p1**-**p4**, **p7**, **p8**, **p10,** and **p11** via the reaction of the methylidyne radical with vinylacetylene through addition of methylidyne to the carbon-carbon double bond and insertion of methylidyne into a hydrogen atom of the CH_2 moiety. Energies calculated at the CCSD(T)-F12/cc-pVTZ-f12// B2PLYPD3/cc-pVTZ + ZPE(B2PLYPD3/cc-pVTZ) level are shown in kJ mol^{-1} and are relative to the energy of the separated reactants.

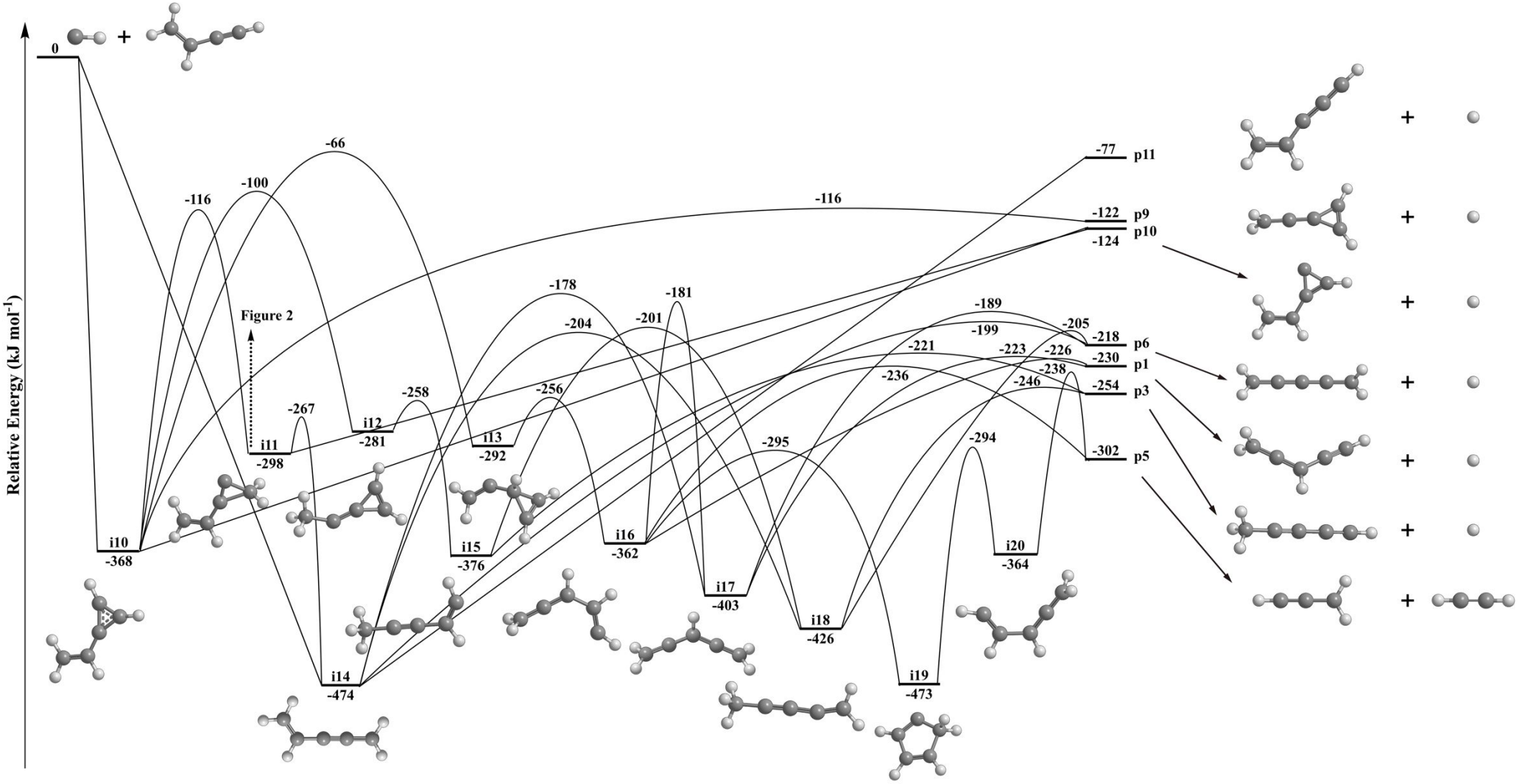

Figure 3. Schematic representation of the portion of C_5H_5 potential energy surface (PES) leading to **p1**, **p3**, **p5**, **p6**, and **p9-p11** via the reaction of the methylidyne radical with vinylacetylene through addition of methylidyne to the carbon-carbon triple bond and insertion into the acetylenic carbon-hydrogen bond. Energies calculated at the CCSD(T)-F12/cc-pVTZ-f12// B2PLYPD3/cc-pVTZ + ZPE(B2PLYPD3/cc-pVTZ) level are shown in kJ mol^{-1} and are relative to the energy of the separated reactants.

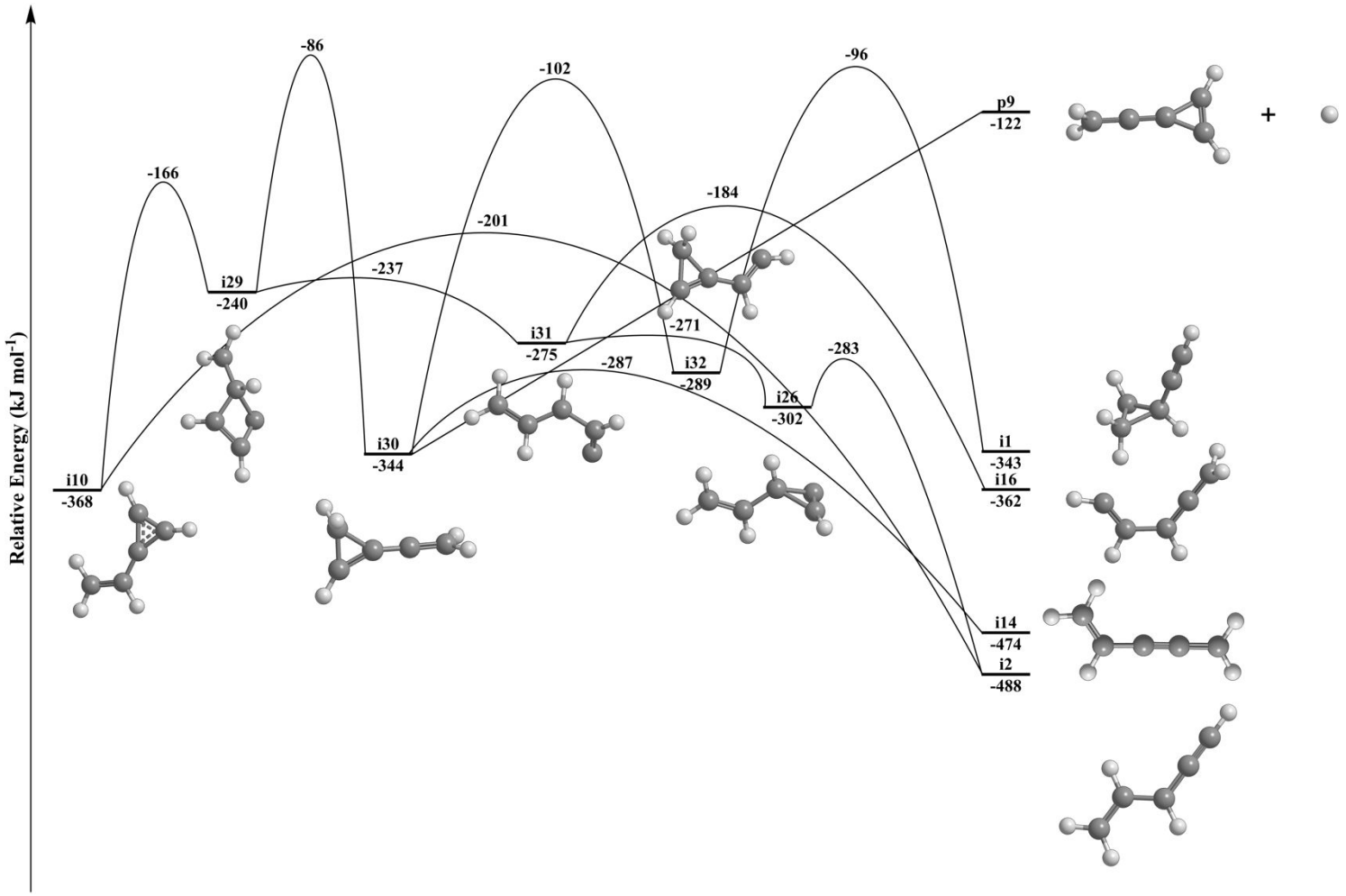

Figure 4. Schematic representation of the portion of C_5H_5 potential energy surface (PES) including **i1**, **i2**, **i10**, **i14**, **i16**, **i26**, **i29-i32,** and **p9** via the reaction of the methylidyne radical with vinylacetylene. Energies calculated at the CCSD(T)-F12/cc-pVTZ-f12// B2PLYPD3/cc-pVTZ + ZPE(B2PLYPD3/cc-pVTZ) level are shown in kJ mol^{-1} and are relative to the energy of the separated reactants.

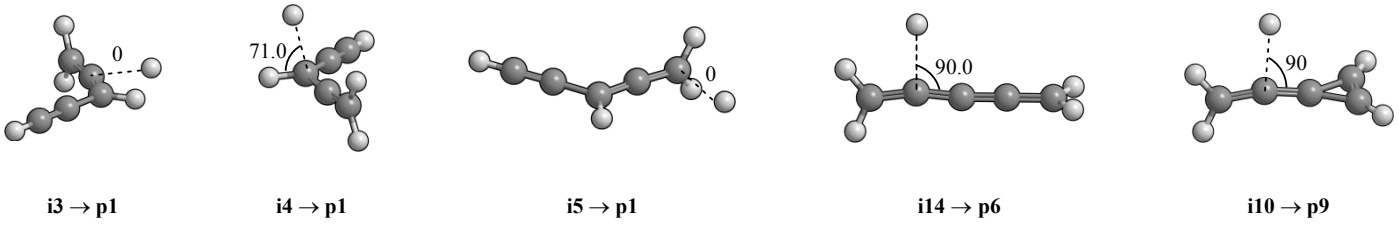

Figure 5. Computed geometries of the selected exit transition states leading to **p1**, **p6**, and **p9**. Angles of the departing hydrogen atoms are given in degrees with respect to the rotation plane of the decomposing complex.

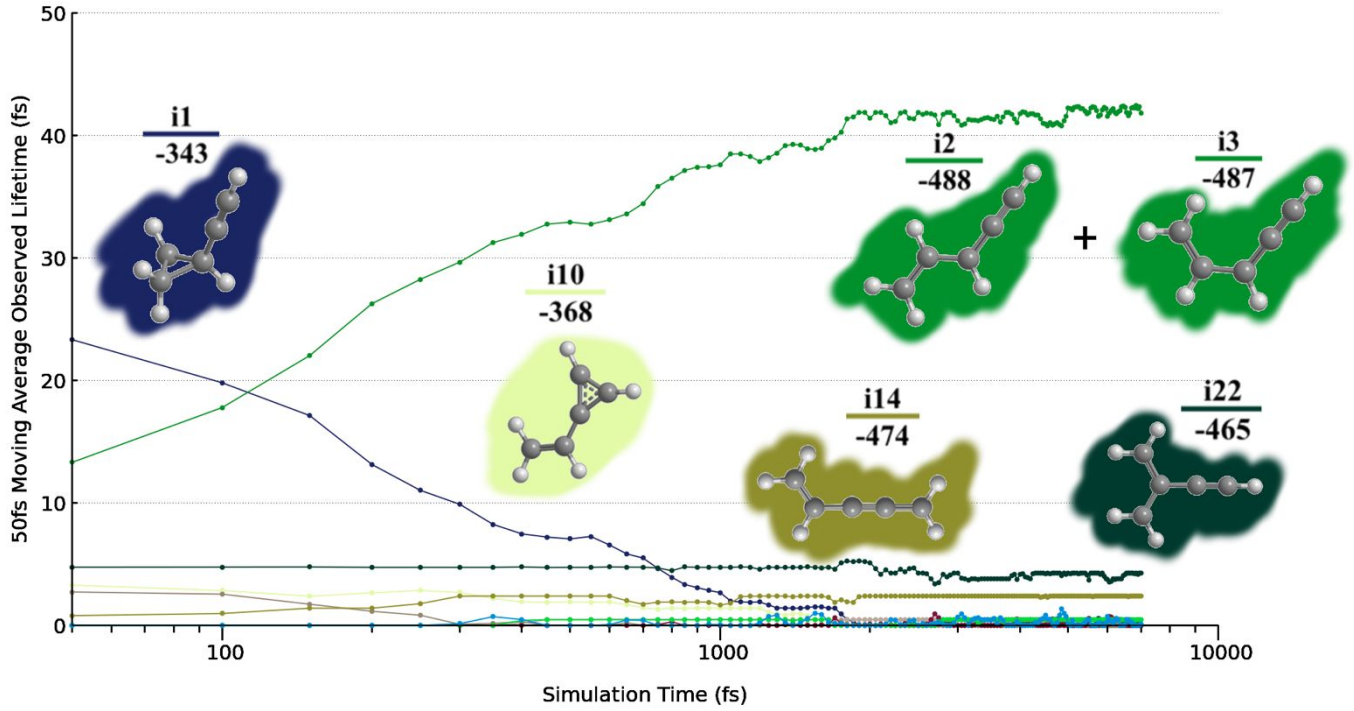

Figure 6. The population of the six most important intermediates after the collision. The x-axis is in log scale. The number under the intermediate name is the relative energy. The population of i2 and i3 are plotted together instead of separately due to their fast interconversion.

Table 1: Peak velocities (v_p) and speed ratios (S) of methylidyne radical (CH; $X^2\Pi$), D1-methylidyne radical (CD; $X^2\Pi$), and vinylacetylene (C_4H_4; X^1A') beams along with the collision energy (E_C) and center-of-mass angle (Θ_{CM}).

beam	v_p (m s^{-1})	S	E_C (kJ mol^{-1})	Θ_{CM} (deg)
CH ($X^2\Pi$)	1867 ± 13	12.6 ± 0.4	20.3 ± 0.3	54.0 ± 0.9
CD ($X^2\Pi$)	1852 ± 9	13.1 ± 0.8	21.2 ± 0.2	52.1 ± 0.9
C_4H_4 ($X\ ^1A'$)	642 ± 20	26.0 ± 1.0		

Table 2. RRKM calculated product branching ratios (in %) for various initial complexes for the collision energies E_C of 20.3 kJ mol^{-1}.

products	RRKM					AIMD
	initial complexes					
	i1	**i2**	**i10**	**i14**	**i22**	
p1	89.58	89.80	88.47	10.13	22.55	75.2
p2	4.10	4.11	4.06	6.69	68.37	10.0
p3	4.26	4.27	4.30	28.18	2.16	4.6
p4	1.21	1.21	1.19	0.39	4.01	1.4
p5	0.28	0.28	0.35	0.15	0.55	3.8
p6	0.06	0.06	0.14	54.46	2.35	2.0
p7	0.37	0.18	0.17	0.00	0.01	0.2
p8	0.10	0.05	0.05	0.00	0.00	0.1
p9	0.04	0.04	1.27	0.00	0.00	2.7
p10	0.00	0.00	0.00	0.00	0.00	0.00
p11	0.00	0.00	0.00	0.00	0.00	0.00